Catalytic Mechanism of Hamster Arylamine *N*-Acetyltransferase 2[†]

Haiqing Wang, Li Liu, Patrick E. Hanna, and Carston R. Wagner*

Department of Medicinal Chemistry, College of Pharmacy, University of Minnesota, Minneapolis, Minnesota 55455

Received November 19, 2004; Revised Manuscript Received June 4, 2005

ABSTRACT: Arylamine *N*-acetyltransferases (NATs) catalyze an acetyl group transfer from AcCoA to primary arylamines, hydrazines, and hydrazides and play a very important role in the metabolism and bioactivation of drugs, carcinogens, and other xenobiotics. The reaction follows a ping-pong bi-bi mechanism. Structure analysis of bacterial NATs revealed a Cys-His-Asp catalytic triad that is strictly conserved in all known NATs. Previously, we have demonstrated by kinetic and isotope effect studies that acetylation of the hamster NAT2 is dependent on a thiolate−imidazolium ion pair (Cys-S^-−His-ImH^+) and not a general acid−base catalysis. In addition, we established that, after formation of the acetylated enzyme intermediate, the active-site imidazole, His-107, is likely deprotonated at physiological pH. In this paper, we report steady-state kinetic studies of NAT2 with two acetyl donors, acetyl coenzyme A (AcCoA) and *p*-nitrophenyl acetate (PNPA), and four arylamine substrates. The pH dependence of k_{cat}/K_{AcCoA} exhibited two inflection points at 5.32 ± 0.13 and 8.48 ± 0.24, respectively. The pK_a at 5.32 is virtually identical with the previously reported pK_a of 5.2 for enzyme acetylation, reaffirming that the first half of the reaction is catalyzed by a thiolate−imidazolium ion pair in the active site. The inflection point at 8.48 indicates that a pH-sensitive group on NAT2 is involved in AcCoA binding. A Brønsted plot constructed by the correlation of log k_4 and log k_{H_2O} with the pK_a for each arylamine substrate and water displays a linear free-energy relationship in the pK_a range from −1.7 (H_2O) to 4.67 (PABA), with a slope of $\beta_{nuc} = 0.80 \pm 0.1$. However, a further increase of the pK_a from 4.67 (PABA) to 5.32 (anisidine) resulted in a 2.5-fold decrease in the k_4 value. Analysis of the pH−k_{cat}/K_{PABA} profile revealed a pK_a of 5.52 ± 0.14 and a solvent kinetic isotope effect (SKIE) of 2.01 ± 0.04 on k_{cat}/K_{PABA}. Normal solvent isotope effects of 4.8 ± 0.1, 3.1 ± 0.1, and 3.2 ± 0.1 on the k_{cat}/K_b for anisidine, pABglu, and PNA, respectively, were also determined. These observations are consistent with a deacetylation mechanism dominated by nucleophilic attack of the thiol ester for arylamines with pK_a values ≤5.5 to deprotonation of a tetrahedral intermediate for arylamines with pK_a values ≥5.5. The general base is likely His-107 because the His-107 to Gln and Asn mutants were found to be devoid of catalytic activity. In contrast, an increase in pH-dependent hydrolysis of the acetylated enzyme was not observed over a pH range of 5.2−7.5. On the basis of these observations, a catalytic mechanism for the acetylation of arylamines by NAT2 is proposed.

Arylamine *N*-acetyltransferases (NATs,[1] EC 2.3.1.5) are phase II metabolism enzymes, which catalyze AcCoA-dependent N-acetylation of arylamines, O-acetylation of arylhydroxylamines, as well as AcCoA-independent N,O-transacetylation of arylhydroxamic acids. The N-acetylation reaction leads to the detoxification of arylamine xenobiotics. The latter two pathways, however, result in bioactivation of arylamine carcinogens, such as 2-aminofluorene, 4-aminobiphenyl, and 2-amino-1-methyl-6-phenylimidazo(4,5-b)-pyridine (PhIP), by the generation of arylamine acetoxy products capable of decomposing into electrophilic arylnitrenium ions. These electrophiles are considered to be the ultimate carcinogens responsible for DNA adduct formation (*1*−*3*).

There are up to three NAT isozymes encoded at distinct gene loci in eukaryotic organisms (*4*). Humans express two functional NAT isozymes, NAT1 and NAT2, which share 81% amino acid sequence identity, but exhibit key differences in substrate specificity and tissue distribution (*5*, *6*). Whereas human NAT2 is expressed predominately in liver and intestinal epithelium (*7*), human NAT1 is more ubiquitously distributed, being found in liver (*8*), bladder (*9*), erythrocytes (*10*), brain (*11*), and skeletal muscle (*12*). Human NAT1 but not human NAT2 has been detected in blastocytes and fetal and neonatal tissues and is postulated

[†] This work was supported by U.S. Public Health Service Grant CA55334 from the National Cancer Institute and a Development Grant in Drug Design from the Department of Medicinal Chemistry, University of Minnesota, Minneapolis, MN.

* To whom correspondence should be addressed: University of Minnesota, Department of Medicinal Chemistry, 8-101 Weaver-Densford Hall, 308 Harvard St., Minneapolis, MN 55455. E-mail: wagne003@tc.umn.edu. Telephone: 651-644-1202.

[1] Abbreviations: AcCoA, acetyl coenzyme A; DMAB, 4-(dimethylamino)benzaldehyde; DTT, dithiothreitol; EDTA, ethylenediaminetetracetic acid; IPTG, isopropyl-β-D-thiogalactopyranoside; LFER, linear free-energy relationship; NAT, arylamine *N*-acetyltransferase; NAT1, hamster monomorphic *N*-acetyltransferase 1; NAT2, hamster polymorphic *N*-acetyltransferase 2; MOPS, 3-(*N*-morpholino)propanesulfonic acid; PAGE, polyacrylamide gel electrophoresis; PE buffer, potassium phophate buffer; PNPA, *p*-nitrophenyl acetate; PABA, *p*-aminobenzoic acid; pABglu, *p*-aminobenzoyl glutamic acid; PNA, *p*-nitroaniline; SDS, sodium dodecyl sulfate; SKIE, solvent kinetic isotope effect; *St*NAT; *Salmonella typhimurium* NAT; TCA, trichloroacetic acid.

10.1021/bi047564q CCC: $30.25
Published on Web 07/29/2005

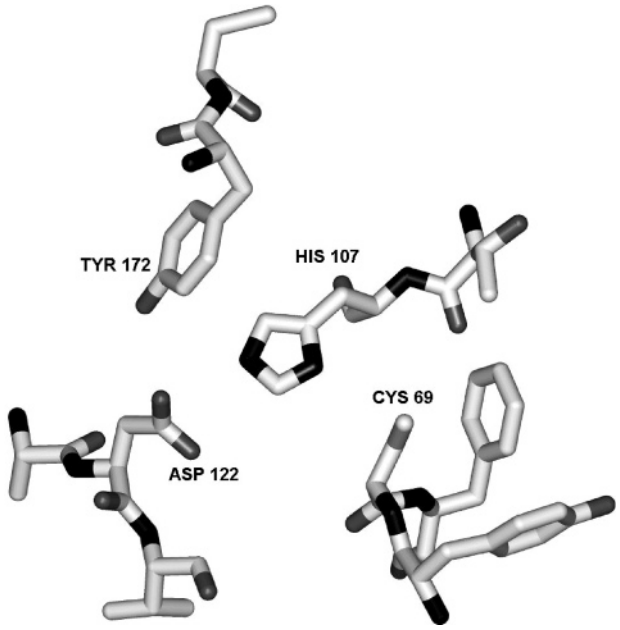

FIGURE 1: X-ray crystallographic structure of the StNAT active site (*21*).

to have endogenous roles in addition to the metabolism of xenobiotics (*13*).

The human NAT1-specific substrates include *p*-aminobenzoic acid (PABA) and *p*-aminosalicylic acid (PAS) (*5*). Unlike the *N*-acetyltransferases in the GNAT superfamily, such as histone *N*-acetyltransferase and serotonin *N*-acetyltransferase, which catalyze the acetylation of either alkylamines or arylakylamines, primary arylamines and hydrazines are the only known substrates for NATs (*14*). The folate catabolism product, *p*-aminobenzoylglutamic acid (pABglu), has recently been suggested as the potential endogenous substrate of human NAT1 (*15*). N-Acetylated pABglu has been reported as a urinary catabolite of folate (*7*, *13*, *16*). The physiological significance of pABglu acetylation remains obscure, because a significant amount of nonacetylated pABglu is also observed. Thus, the role of human NAT1 as a folate metabolism enzyme is not clear.

To better understand the biology of human NAT1, it is necessary to elucidate in detail its substrate specificity and molecular mechanism. Hamster NATs have been proven to be useful models for human NATs (*17*, *18*), with human NAT1 and hamster NAT2 having 82% sequence identity and similar substrate selectivity (*19*). Recently, we reported kinetic studies on hamster NAT2 and demonstrated that the catalytic mechanism depends on the formation of a thiolate−imidazolium ion pair (*20*). Although a cysteine protease-like catalytic triad of Cys-68, His-107, and Asp-122 is conserved in all NATs (Figure 1) (*21*−*23*), the catalytic mechanisms of hamster NAT2 and cysteine proteases were found to diverge. Studies of the inactivation of NAT2 with neutral and anionic cysteine-specific alkylation agents revealed a nonpolar active-site environment. The formation of a thiolate−imidazolium ion pair by Cys-68 and His-107 with an apparent pK_a of 5.2 was found to be catalytically essential. Consequently, acetylation of the enzyme by either AcCoA or an alternative acetylation substrate, *p*-nitrophenyl acetate (PNPA), does not involve general acid catalysis. Mutagenic studies suggested that Asp-122 of the catalytic triad, which is presumably involved in ionic interaction with the imidazolium of His-107, is critical for structural integrity and catalytic activity of the enzyme. In addition, the enzyme thiol ester intermediate was found to be highly stable in aqueous media, with a half-life of 88 s at 25 °C (*20*).

To further elucidate the catalytic mechanism of hamster NAT2, we have investigated the acetylation and deacetylation of hamster NAT2 by steady-state kinetic studies. The kinetic parameters were determined for natural substrates as well as a number of alternative substrates, providing insights into the substrate specificity of this enzyme. On the basis of Brønsted plot analysis, pH-dependence studies, and solvent kinetic isotope effects (SKIEs), we propose a catalytic mechanism for the transacetylase reaction.

MATERIALS AND METHODS

Materials. AcCoA, anisidine, DMAB, MOPS, PNPA, PNA, PABA, pABglu, dimethylglutaric acid, and pyrophosphoric acid were purchased from Sigma−Aldrich (St. Louis, MO). TCA and DTT were purchased from Fisher Scientific, Inc. (Pittsburgh, PA). BL21Codon Plus (RIL) competent *Escherichia coli* cells were purchased from Stratagene (La Jolla, CA). Rosetta supercompetent *E. coli* cells and the Protein Refolding kit were purchased from Novagen (Madison, WI). DEAE Sepharose Fast Flow anion-exchange resin was purchased from Amersham Pharmacia (Ann Arbor, MI). The protein concentration was determined with the Bradford assay (*24*). Spectrophotometric data were collected with a Varian (Palo Alto, CA) Cary 50 UV−vis spectrophotometer. Kinetic data were analyzed with the JMP IN software suite (SAS Institute, Inc.)

Expression and Purification of Hamster Recombinant NAT2. Expression construct plasmid pPH70D, which contains the hamster NAT2 cDNA, has been reported (*25*). The pPH70D vector was transformed into competent BL-21 Codon Plus RIL *E. coli* cells according to the protocol of the manufacturer. Overnight cultures (10 mL) were grown from single colonies and were diluted 100-fold into 1 L of Terrific Broth (TB) containing ampicillin (100 μg/mL) and chloramphenicol (50 μg/mL) in a 2 L flask. Cultures were grown aerobically with shaking at 250 rpm at 37 °C until the $OD_{600\ nm}$ was 0.4, at which time IPTG was added to a final concentration of 0.2 mM. After additional growth for 8 h, the cells were harvested by centrifugation at 5000*g* for 15 min at 4 °C. The cell pellets were quick-frozen in a dry ice−acetone bath and stored at − 80 °C. NAT2 was purified as previously described except that DEAE Sepharose Fast Flow anion-exchange resin was used (*25*).

Site-Directed Mutagenesis. Site-directed mutagenesis of the NAT2 catalytic triad His-107 to Gln (H107Q) and to Asn (H107N) was carried out with the pPH70D vector and QuickChange site-directed mutagenesis kit (Stratagene, La Jolla, CA). The oligonucleotide primer used for H107Q was 5′-G TAC AGC AGT GGT ATG ATT CAA CTT CTA GTA CAG GTG ACC-3′, and the oligonucleotide primer used for H107N was 5′-G TAC AGC AGT GGT ATG ATT AAT CTT CTA GTA CAG GTG ACC-3′. Mutant DNA was fully sequenced by automated sequencing, thus ensuring that no additional mutations had been incorporated. The mutated plasmids were transformed to Rosetta *E. coli* cells and BL-21 Codon Plus (RIL) *E. coli* cells according to the instructions of the supplier.

Expression of H107Q and H107N Mutant Proteins. The expression levels of H107Q and H107N mutant proteins were examined in both BL21(RIL) *E. coli* cells and Rosetta *E. coli* cells and under various growth conditions. Overnight cultures (100 mL) were grown from single colonies, and 10 mL of the cultures were inoculated to 1 L of LB media containing ampicillin (final concentration of 100 μg/mL) and chloramphenicol (final concentration of 50 μg/mL). Cultures were grown aerobically at 37 or 25 °C to an OD_{600} of 0.4 or 1.0, at which time IPTG was added to a final concentration of 200 μM. After incubation for an additional 1−5 h, the cells were harvested by centrifugation at 5000*g* for 15 min at 4 °C. The cells were lysed as previously described (*20*). The mutant proteins in the inclusion bodies were resolubilized with a Protein Refolding kit (Novagen). More than 90% of the mutant proteins were resolubilized after extensive dialysis in Tris buffer (20 mM at pH 8.0 and 1 mM DTT) and DEAE column purification. Control experiments were conducted under the same conditions with insoluble protein generated during the expression of wild-type NAT2.

NAT2 Activity Assay. The assay was carried out with PNPA as the acetyl donor and PABA as the acetyl acceptor. The assay mixtures contained NAT2 (0.5 μg/mL, 14.6 nM), PABA (0.5 mM), PNPA (2 mM), and MOPS buffer (100 mM at pH 7.0, 150 mM NaCl, and 0.1 mM DTT) in a final volume of 500 μL. Incubations were conducted at 25 °C in 1.5 mL acryl cuvettes with a Varian Cary 50 UV−vis spectrophotometer equipped with a circulating water bath. The reaction was initiated by addition of PNPA dissolved in DMSO (10 μL). DMSO did not affect enzyme activity at concentrations less than 5%. The rate of the reaction was determined by monitoring the linear increase in absorbance at 400 nm because of the formation of *p*-nitrophenol ($\epsilon_{400\ nm}$ = 9400 M^{-1} cm^{-1}). The results were corrected for nonenzymatic hydrolysis of PNPA by conducting the reaction in the absence of enzyme. The specific activity was expressed as micromoles of product formed per milligram of protein per minute.

Steady-State Kinetics. The assays were conducted with PNPA or AcCoA as the acetyl donor and one of the following primary arylamines as the acetyl acceptor: anisidine, PABA, pABglu, or PNA. The kinetic assays were carried out at various concentrations of one substrate in the presence of a fixed concentration of the other substrate. Initial velocities were determined with six different concentrations of each substrate. All of the kinetic assays were performed in triplicate at 25 °C.

The initial velocities of the reactions with PNPA/anisidine, PNPA/PABA, and PNPA/pABglu were measured as described for the NAT2 activity assay. In a final volume of 500 μL, NAT2 (0.3 μg/mL, 8.76 nM) was incubated with either anisidine (0.025−1 mM), PABA (0.025−1.2 mM), or pABglu (0.5−10 mM) and PNPA (0.5−8 mM) in MOPS buffer (100 mM at pH 7.0, 150 mM NaCl, and 0.1 mM DTT). The reactions were initiated by addition of PNPA dissolved in DMSO (20 μL). The final concentration of DMSO was 4%. The reactions were monitored continuously as a linear increase in absorbance at 400 nm. The results were corrected for the nonenzymatic PNPA hydrolysis by conducting the reaction in the absence of enzyme.

The initial velocity of the reaction with AcCoA/PABA was measured as a linear decrease of the PABA concentration. In a final volume of 1 mL, NAT2 (0.3 μg/mL, 8.76 nM) was incubated with PABA (0.03−0.24 mM) and AcCoA (0.5−8 mM) in dimethylglutaric acid buffer (50 mM at pH 7.0, 80 mM NaCl, and 0.1 mM DTT). The reactions were initiated by addition of AcCoA dissolved in the same buffer without DTT (100 μL). Aliquots (20−60 μL) were withdrawn at 10 s intervals (0−180 s) and transferred to an assay mixture containing TCA (4%, w/v), DMAB (2.5%, w/v), and acetonitrile (45%, v/v) (final volume of 300 μL). The unreacted PABA was quantified by measuring the absorbance at 450 nm ($\epsilon_{450\ nm}$ = 15 900 M^{-1} cm^{-1}) (*26*).

The initial velocity of the reaction with AcCoA/pABglu was measured as a linear decrease of the pABglu concentration. In a final volume of 1 mL, NAT2 (3 μg/mL, 87.6 nM) was incubated with pABglu (0.8−3 mM) and AcCoA (0.2−3 mM) in dimethylglutaric acid buffer (50 mM at pH 7.0, 80 mM NaCl, and 0.1 mM DTT). The reactions were initiated by addition of AcCoA dissolved in H_2O (20 μL). Aliquots (25−40 μL) were withdrawn at 30 s intervals (0−300 s) and transferred to an assay mixture containing TCA (4%, w/v), DMAB (2.5%, w/v), and acetonitrile (45%, v/v) (final volume of 400 μL). The remaining pABglu was quantified by measuring the absorbance at 495 nm ($\epsilon_{495\ nm}$ = 5040 M^{-1} cm^{-1}) (*26*).

The initial velocity of the reaction with AcCoA/PNA was measured as a linear decrease in the absorbance at either 430 or 440 nm because of the acetylation of PNA ($\epsilon_{430\ nm}$ = 3040 M^{-1} cm^{-1} and $\epsilon_{440\ nm}$ = 1600 M^{-1} cm^{-1}). The reactions were initiated by the addition of AcCoA (10 μL) to NAT2 and PNA in dimethylglutaric acid buffer (50 mM, 80 mM NaCl, and 0.1 mM DTT at pH 7.0) (final volume of 300 μL). Assay mixtures contained NAT2 (50 μg/mL, 1.46 μM), AcCoA (0.04−0.8 mM), and PNA (0.5−2.5 mM). The reactions were monitored over a maximum of 5 min.

Reversible Inhibition of NAT2 by AcPABA. To determine the inhibitory effect of AcPABA on the free enzyme, NAT2 activity was assayed with 2 mM PNA and various concentrations of AcCoA (60−400 μM); similarly, to determine the inhibitory effect on the acetylated enzyme, 200 μM AcCoA and various concentrations of PNA (0.5−2 mM) were used in the assays. The assays were carried out as described for steady-state kinetics with AcCoA/PNA as the substrate pair, except AcPABA (0−3.33 mM) was included in the incubation mixture.

pH Profiles of NAT2-Catalyzed Transacetylation Reactions with AcCoA and PABA. At pH values ranging from 5 to 10.0, the kinetic parameters, k_{cat}/K_{AcCoA}, K_{AcCoA}, and k_{cat}, were determined at saturating levels of PABA (400−600 μM), while varying the AcCoA concentrations (2−24 mM). Either dimethylglutaric acid buffer (50 mM at pH 5.0−7.0, 0.1 mM DTT, and 1% glycerol) or pyrophosphoric acid buffer (50 mM at pH 8.0−10.0, 0.1 mM DTT, and 1% glycerol) was employed in the assay. The ionic strength was maintained at 150 mM with NaCl. Assays were performed as described for the steady-state kinetics.

pL Profile of NAT2-Catalyzed Transacetylation Reactions with PNPA and PABA. The kinetic parameter, k_{cat}/K_{PABA}, was determined at a fixed concentration of PNPA (2 mM) and six concentrations of PABA (20−240 μM) over a pL range of 5.2−9.0. Buffers were prepared in H_2O and D_2O in parallel. The values of pD for the D_2O buffers were corrected according to the formula pD = meter reading + 0.4 and

were adjusted with DCl and NaOD (*27*). Final reaction mixtures contained 98% D_2O. For the pL range of 5.2−7.0, dimethylglutaric acid buffer (50 mM, 0.1 mM DTT, and 1% glycerol) was used; for the pL range of 7.5−9.0, Tris buffer (50 mM, 0.1 mM DTT, and 1% glycerol) was used. The ionic strength was held constant at 150 mM with NaCl. Assays were performed as described in the steady-state kinetics, except that the formation of *p*-nitrophenol was monitored at the isosbestic point of 349 nm ($\epsilon = 6700\ M^{-1}\ cm^{-1}$) (*28*).

pH Profile of Acetyl−Enzyme Hydrolysis. The rate of acetyl−enzyme hydrolysis was determined with PNPA as the acetyl donor. At pH values ranging from 5.2 to 9.0, NAT2 (8 μM, 274 μg/mL) was incubated with PNPA (320 μM) in either dimethylglutaric acid buffer (pH 5.0−7.0) or Tris buffer (pH 7.5−9.0) in a final volume of 500 μL. The buffers were prepared as described above, and the ionic strength was held constant at 150 mM with NaCl. The reactions were initiated by adding PNPA dissolved in DMSO (10 μL). The rates of acetyl−enzyme hydrolysis were determined by monitoring the increase in absorbance at 349 nm ($\epsilon = 6700\ M^{-1}\ cm^{-1}$) because of the formation of *p*-nitrophenol (*28*). The results were corrected for nonenzymatic hydrolysis of PNPA by measuring the rate of the reaction in the absence of enzyme.

SKIE on the Deacetylation of Acetyl−Enzyme by Anisidine, pABglu, and PNA. The SKIE on the decetylation reaction was examined at pL 7.0 in dimethylglutaric acid buffer (50 mM, 80 mM NaCl, and 0.1 mM DTT) prepared in H_2O and D_2O in parallel. The kinetic parameters, k_{cat}/K_{pABglu} and $k_{cat}/K_{anisidine}$, were determined at a fixed concentration of PNPA (2 mM) and five different concentrations of anisidine (0.025−0.8 mM) and pABglu (0.125−2 mM), and k_{cat}/K_{PNA} was determined at a fixed concentration of AcCoA (400 μM) and five different concentrations of PNA (50−700 μM). The reactions were carried out as described for the steady-state kinetic analysis. The assays performed in D_2O buffer contained 98% D_2O.

pK_a of the Aniline Group of pABglu. The pK_a was determined by monitoring the change in absorbance at 274 nm as a function of pH (*29*). The absorbance of pABglu was measured over a pH range of 1.4−5.1 in KCl buffer (50 mM at pH 1.4−2.0), glycine buffer (50 mM at pH 2.25−3.5), and dimethylglutaric acid buffer (50 mM at pH 4−5.1). Plotting the absorbance intensity versus pH revealed a single sigmodial curve. The pK_a value was calculated by fitting the data to the formula, $Abs_{274\ nm} = C/[1 + 10^{(pH-pK_a)}]$, where C is a pH-independent constant.

Kinetic Data Analysis. The initial velocities from steady-state kinetics were analyzed by Lineweaver−Burk plots and fit to eq 1 (Scheme 1) by a nonlinear regression approach with JMP IN software suite (SAS Institute, Inc.). [A] and [B] in eq 1 represent the concentration of acetyl donor and acceptor; K_a represents either K_{PNPA} or K_{AcCoA}; and K_b represents either K_{PABA}, $K_{anisidine}$, K_{pABglu}, or K_{PNA}. When PNPA was used as the acetyl donor, the reaction pathway is shown in Scheme 1. The steady-state rate expressions for K_a, K_b, and k_{cat} are shown in eqs 2−4. When AcCoA was used as the acetyl donor, the reaction pathway is shown in Scheme 2. The expressions for K_a, K_b, and k_{cat} are shown in eqs 7−9, where K_m^a and K_m^b represent the Michaelis−Menten constants for substrates A and B in the first half and second half of the reaction, respectively. The Lineweaver−Burk plots for the inhibition of NAT2 with AcPABA revealed that AcPABA is an uncompetitive inhibitor of the free enzyme and a competitive inhibitor of the acetyl−enzyme. Therefore, the inhibition data were fit to eq 13, which is the reciprocal form of eq 12. The (K_b/V_{max})app in eq 14 was obtained as the slope of eq 13 at each concentration of the inhibitor. The K_I was determined by plotting the concentration ([I]) versus (K_b/V_{max})app (eq 14)

Scheme 1

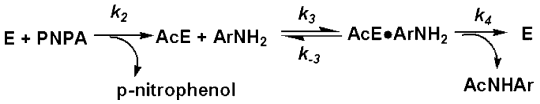

$$V = \frac{V_{max}[A][B]}{K_a[B] + K_b[A] + [A][B]} \quad (1)$$

$$k_{cat} = V_{max}/[E_t] = k_4 \quad (2)$$

$$K_a = \frac{k_4}{k_2} \quad (3)$$

$$K_b = \frac{k_{-3} + k_4}{k_3} = K_m^b \quad (4)$$

$$\frac{k_{cat}}{K_b} = \frac{k_4}{K_m^b} \quad (5)$$

$$\frac{k_{cat}}{K_a} = k_2 \quad (6)$$

Scheme 2

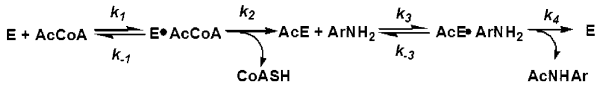

$$V = \frac{V_{max}[A][B]}{K_a[B] + K_b[A] + [A][B]} \quad (1)$$

$$k_{cat} = V_{max}/[E_t] = \frac{k_2 k_4}{k_2 + k_4} \quad (7)$$

$$K_a = \frac{k_{-1} + k_2}{k_1} \times \frac{k_4}{k_2 + k_4} = K_m^a \times \frac{k_4}{k_2 + k_4} \quad (8)$$

$$K_b = \frac{k_{-3} + k_4}{k_3} \times \frac{k_2}{k_2 + k_4} = K_m^b \times \frac{k_2}{k_2 + k_4} \quad (9)$$

$$\frac{k_{cat}}{K_a} = \frac{k_2}{K_m^a} \quad (10)$$

$$\frac{k_{cat}}{K_b} = \frac{k_4}{K_m^b} \quad (11)$$

$$V = \frac{V_{max}[A][B]}{K_a[B] + K_b(1 + [I]/K_I)[A] + [A][B]} \quad (12)$$

$$\frac{1}{V} = \frac{K_b(1 + [I]/K_I)}{V_{max}[B]} + \frac{K_a}{V_{max}[A]} + \frac{1}{V_{max}} \quad (13)$$

$$\left(\frac{K_b}{V_{max}}\right)_{app} = \frac{K_b(1 + [I]/K_I)}{V_{max}} \quad (14)$$

pH profile data were analyzed by nonlinear regression with the JMP IN software suite (SAS Institute, Inc.). The pH-

dependent k_{cat} values were fit to eq 15, where $(k_{cat})_{lim}$ is the pH-independent plateau value. The pH$-k_{cat}/K_{PABA}$ curve was fit to eq 16 according to a mechanism involving one pH-sensitive group. Deprotonation of the group causes an increase of k_{cat}/K_{PABA} from $(k_{cat}/K_{PABA})_{lim}'$ to $(k_{cat}/K_{PABA})_{lim}$. The reciprocal of the fold of increase is represented as r ($r < 1$). The pH$-k_{cat}/K_{AcCoA}$ was fit to eq 17 according to a mechanism involving two pH-sensitive groups. The k_{cat}/K_{AcCoA} reaches $(k_{cat}/K_{AcCoA})_{lim}$ when only one group is deprotonated and becomes $(k_{cat}/K_{AcCoA})_{lim}'$ when both groups are deprotonated. The value of $(k_{cat}/K_{AcCoA})_{lim}'$ equals $r(k_{cat}/K_{AcCoA})_{lim}$ with $r < 1$. The pH$-K_{AcCoA}$ was fit to eq 18, which is mechanistically similar to eq 16

$$k_{cat} = \frac{(k_{cat})_{lim}}{1 + 10^{(pK_a - pH)}} \quad (15)$$

$$k_{cat}/K_{PABA} = \frac{(k_{cat}/K_{PABA})_{lim}(1 + r10^{(pK_a - pH)})}{1 + 10^{pK_a - pH}} \quad (16)$$

$$k_{cat}/K_{AcCoA} = \frac{(k_{cat}/K_{AcCoA})_{lim}(1 + r10^{(pH - pK_{a2})})}{(1 + 10^{(pH - pK_{a2})} + 10^{(pK_{a1} - pH)})} \quad (17)$$

$$K_{AcCoA} = \frac{(K_{AcCoA})_{lim}(1 + r10^{(pK_a - pH)})}{1 + 10^{pK_a - pH}} \quad (18)$$

RESULTS

Determination of Steady-State Kinetic Parameters. Steady-state kinetic studies of NAT2 were carried out with two acetyl donors, PNPA and AcCoA, and four acetyl acceptors, anisidine, PABA, pABglu, and PNA (Figure 2). Initial velocities were determined at pH 7.0 and six different substrate concentrations. Lineweaver−Burk analysis of the initial velocities as a function of substrate concentrations revealed parallel lines, consistent with a ping-pong bi-bi kinetic mechanism. The data were fit with eq 1 using nonlinear regression analysis, and the kinetic parameters, K_a, K_b, and k_{cat}, were determined (Table 1).

Previous stopped-flow kinetics of NAT2 with PNPA suggested that the acetylation reaction presumably follows a bimolecular reaction pathway without the formation of a stable Michaelis−Menten complex (E·PNPA) (*20*). The transacetylation reactions with PNPA and various arylamines are shown in Scheme 1, where AcE is the acetyl−enzyme intermediate. Application of the steady-state approximation to the concentration of the AcE·$ArNH_2$ complex yields eq 1. Because the rate of acetylation (k_2[PNPA]) is proportional to the concentration of PNPA, the maximum rate constant for the overall reaction (k_{cat}) is dependent on the deacetylation rate constant (k_4) (eq 2). Therefore, the k_4 values for anisidine, PABA, and pABglu are equivalent to the k_{cat} values, which are 260 ± 20, 620 ± 40, and 120 ± 3 s^{-1}, respectively (Table 1). In eq 4, K_b represents the Michaelis−Menten constant (K_m^b) for the acetyl acceptor. The ratio of k_{cat}/K_a revealed a second-order rate constant (k_2) for PNPA acetylation (eq 6). On the basis of the ping-pong mechanism, the first substrate can undergo the acetylation reaction without the presence of a second substrate. Therefore, the k_2 for PNPA is expected to be independent of the various arylamine acetyl acceptors. The k_{cat}/K_a values for PNPA produced from the steady-state

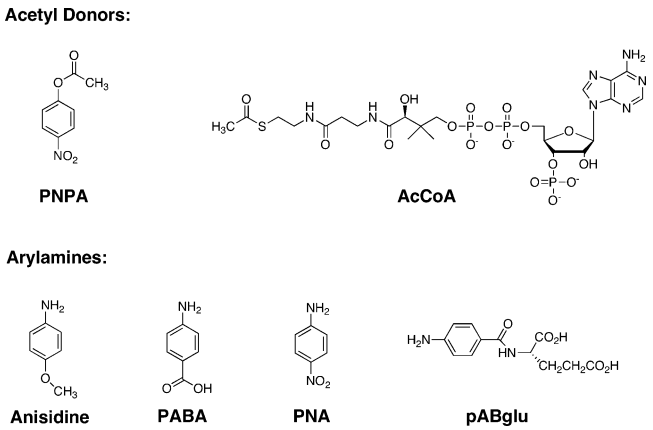

FIGURE 2: Chemcial structures of acetyl donors (A) and acetyl acceptors (B).

kinetic analysis with three arylamines are indeed very similar and lie in the range of 62−100 mM^{-1} s^{-1}. These results are close approximations of the second-order rate constant, 140 mM^{-1} s^{-1}, determined previously by stopped-flow kinetic studies of enzyme acetylation by PNPA (*20*).

The transacetylation reactions with AcCoA as the acetyl donor employ a typical ping-pong bi-bi mechanism that involves two reversible substrate-binding steps along with two chemical reactions as outlined in Scheme 2. Although Scheme 2 exhibits an identical steady-state rate equation (eq 1) as Scheme 1, the expressions for the kinetic parameters (K_a, K_b, and k_{cat}) differ for AcCoA-mediated acetylation (eqs 7−9). In Scheme 2, the k_{cat} is determined by the individual rate constants for both the acetylation (k_2) and deacetylation (k_4) steps (eq 7). Because the values of k_4 and K_m^b for PABA can be inferred from the previous studies of PNPA acetylation, the value of k_2 for AcCoA is predicted to be in the range of 298−651 s^{-1} (eqs 7 and 9), with an average of 475 s^{-1}. As a result, the k_2 for AcCoA is comparable to the k_4 for anisidine, PABA, and pABglu, indicating that both the acetylation and deacetylation steps are partially rate-limiting. Nevertheless, the k_2 for AcCoA is nearly 800-fold higher than the overall steady-state rate (k_{cat} of 0.60 ± 0.02 s^{-1}) at saturating concentrations of PNA, suggesting that the deacetylation step is rate-limiting. The k_{cat} of 0.60 ± 0.02 s^{-1} is, therefore, a close approximation of the k_4 for PNA. Different K_a values for AcCoA were obtained from the reactions with various acetyl acceptors, suggesting that K_a is dependent upon the Michaelis−Menten constant for AcCoA (K_m^b) as well as the factor $k_4/(k_2 + k_4)$ (eq 8). Incorporating the values of k_2 and k_4 in eq 8 yielded a K_m^a of 5.94 mM for AcCoA, indicating that AcCoA has low affinity for NAT2. Similar to the expression for the K_a (eq 8), the K_b for PNA is dependent on the Michaelis−Menten constant for PNA (K_m^a) and the factor $k_2/(k_2 + k_4)$ (eq 9). Because the k_2 for AcCoA is much greater than the k_4 for PNA, the value of $k_2/(k_2 + k_4)$ is close to unity. Thus, assuming k_{-3} and $k_3 \gg k_4$, the K_m^b is nearly identical to the K_b (0.77 ± 0.06 mM), subsequently, K_m^b for PNA will approximate the dissociation constant for PNA (0.77 mM). Further, because of the very small value of k_4, a significantly smaller value for K_a was determined for PNA, compared to the other substrates; the K_a calculated for AcCoA is also smaller, while the k_{cat}/K_a value for PNA remained similar to that observed for PABA or pABglu. In contrast, for the other

Table 1: Steady-State Kinetic Parameters for Acetyl Donors and Acceptors

acetyl donor	acetyl acceptor	K_a (mM)	K_b (mM)	k_{cat} (s^{-1})	k_{cat}/K_a[a] (s^{-1} mM^{-1})	k_{cat}/K_b[a] (s^{-1} mM^{-1})
PNPA	anisidine	2.8 ± 0.4	0.34 ± 0.04[b]	260 ± 20[b]	100 ± 20	790 ± 120
PNPA	PABA	10 ± 1	0.23 ± 0.02[b]	620 ± 40[b]	62 ± 9	2700 ± 400
PNPA	pABglu	1.5 ± 0.1	1.7 ± 0.1[b]	120 ± 3[b]	80 ± 6	70 ± 5
AcCoA	PNA	0.037 ± 0.003	0.77 ± 0.06[c]	0.60 ± 0.02[c]	16 ± 2	0.780 ± 0.08
AcCoA	PABA	3.4 ± 0.3	0.12 ± 0.01	200 ± 1	60 ± 6	1700 ± 200
AcCoA	pABglu	1.2 ± 0.2	2.4 ± 0.3	76 ± 6	60 ± 10	32 ± 6

[a] k_{cat}/K_a and k_{cat}/K_b values were calculated from k_{cat}, K_a, and K_b. [b] $K_b = K_m^b$ (eq 4), and $k_{cat} = k_4$ (eq 2). [c] The deacetylation step is rate-limiting ($k_2 \gg k_4$). $K_b = K_m^b$ (eq 9), and $k_{cat} = k_4$ (eq 7). Details are described in the Results.

arylamine substrates, the value of k_4 is considerably larger and similar to k_2. Therefore, the value for K_m^b will not be equivalent to the substrate dissociation constant. Nevertheless, regardless of the acetyl donors, substrate specificities can be represented by the value of k_{cat}/K_b, which, in both cases, is equivalent to k_4/K_m^b (eqs 5 and 11) Clearly, PABA is the preferred substrate with k_{cat}/K_b that is 2180-, 39−53-, and 3.4-fold greater than the value for PNA, pABglu, and anisidine, respectively.

Product Inhibition Studies. In Schemes 1 and 2, it is assumed that, once the product is formed, it diffuses out of the enzyme active site without the formation of a stable enzyme−product complex. This assumption is supported by the results from the product inhibition studies carried out with AcPABA and CoASH. AcPABA exhibited uncompetitive inhibition with respect to the acetyl donor (AcCoA) (Figure 3A) and competitive inhibition versus the acceptor amine (PNA) (Figure 3B). A K_I of 1.94 mM was calculated from the Lineweaver−Burk plot (inset of Figure 3B). This type of inhibition and the resulting K_I value suggest that AcPABA has modest affinity with the acetyl−enzyme intermediate at the enzyme active site but no significant affinity with the free enzyme. No inhibition of NAT2 was observed within the CoASH concentration range (1−8 mM) (data not shown). Therefore, it is very unlikely that the acetylation and deacetylation rate constants (k_2 and k_4) are influenced by the product-release steps, implying that the values of k_2 and k_4 reflect the chemical reactivity of the reactants.

Brønsted Plot for the Deacetylation Reaction. The deacetylation rate constant (k_4) for PNA is significantly lower (1000-, 430-, and 200-fold) than that for PABA, anisidine, and pABglu. This is not unexpected because the nitro moiety at the para position of aniline is a stronger electron-withdrawing group when compared to a methoxy or a carboxylic acid moiety. Therefore, the nucleophilicity of the acceptor amine may contribute to the rate of the deacetylation reaction. Further evidence is provided by the previous kinetic studies of the acetyl−enzyme hydrolysis, which demonstrated that the acetyl−enzyme intermediate is relatively stable in the absence of arylamine substrates (*20*). The k_{H_2O}, referred to as the rate constant of hydrolysis of the acetyl−enzyme, was determined to be 7.85×10^{-3} s^{-1} at pH 7.0, approximately 80-fold lower than the k_4 for PNA. Apparently, the slow hydrolysis rate is at least in part due to the poor nucleophilicity of H_2O, where the $pK_{H_3O^+}$ of −1.7 is lower than the $pK_{NH_3^+}$ of 1.0 for PNA. The $pK_{NH_3^+}$ of pABglu was determined to be 2.93 by measuring the pH-dependent absorbance change at 274 nm because of the protonation state of the aniline group (*29*). This determined $pK_{NH_3^+}$ value, along with the reported $pK_{NH_3^+}$ and $pK_{H_3O^+}$ values for the other acetyl acceptors (*30*), was plotted versus the corresponding $\log(k_4)$ [or $\log(k_{H_2O})$] values (Figure 4). The Brønsted plot features a linear increase of $\log(k_4)$ [or $\log(k_{H_2O})$] for the $pK_{NH_3^+}$ (or $pK_{H_3O^+}$) range from −1.7 to 4.67, with a large positive slope (β_{nuc}) of 0.8 ± 0.1. This β_{nuc} value suggests that the deacetylation step is initiated through the nucleophilic attack at the thiolester, generating a positive charge on the attacking nucleophile in the tetrahedral transition state. However, as the $pK_{NH_3^+}$ increases for an additional 0.67 unit from 4.67 to 5.34, the $\log(k_4)$ decreases slightly, corresponding to a 2.5-fold decrease in k_4. These data suggest that a further increase in the nucleophilicity of the substrate results in a change in the reaction mechanism during deacetylation.

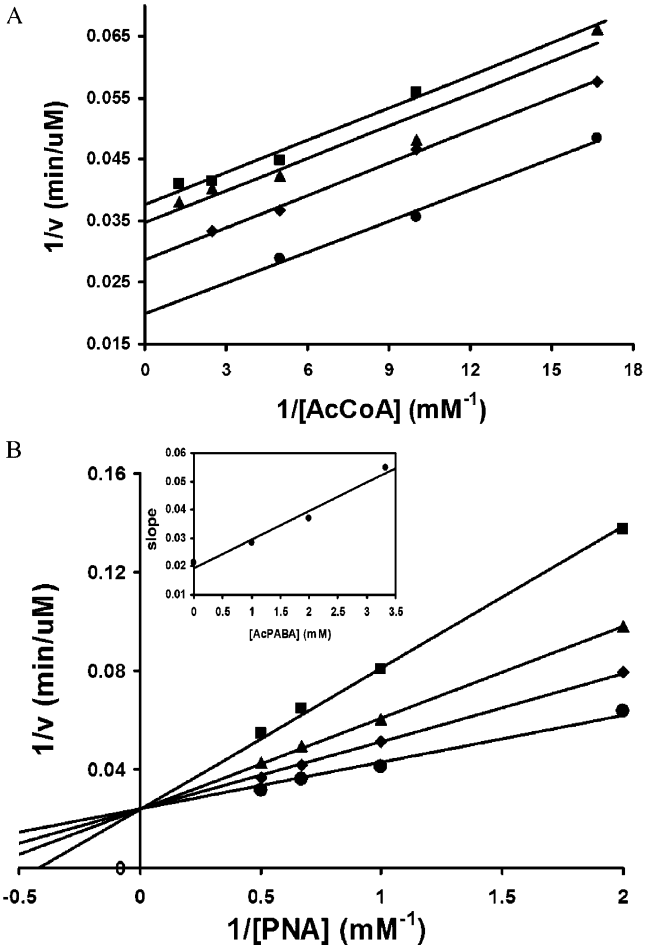

FIGURE 3: Lineweaver−Burk plots of the uncompetitive inhibition of NAT2 (A) and the competitive inhibition of the acetylated enzyme (B) by AcPABA 3.33 mM (■), 2 mM (◆), 1 mM (▲), and control (●) (eq 13). Inset, plot of the slopes of the lines in B against the corresponding AcPABA concentrations. $K_I = 1.94 \pm 0.1$ mM is derived from the slope of the line (eq 14).

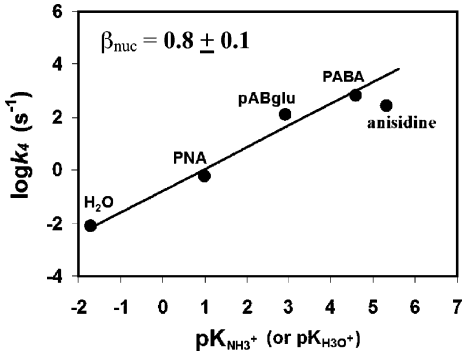

FIGURE 4: Brønsted plot of the deacetylation rate constants for the acetyl−enzyme with various arylamine substrates (k_4) and H_2O (k_{H_2O}). Linear regression of the data resulted in the line with the slope $\beta_{nuc} = 0.8 \pm 0.1$.

Effect of pH on Steady-State Kinetics. The catalytic mechanism for the acetylation reaction has been reported (*20*). The reaction was found to be dependent on the highly reactive Cys-68 residue at the active site. Under both neutral and basic conditions, the Cys-68 is presumably activated by the active-site His-107 through the formation of a thiolate−imidazolium ion pair. The apparent pK_a for the thiolate−imidazolium ion pair was determined to be 5.2. To delineate the catalytic mechanism for the overall reaction pathway, particularly the deacetylation step, pH-dependent steady-state kinetics was carried out with both AcCoA/PABA and PNPA/PABA substrate pairs.

The pH dependence of the transacetylation reaction with AcCoA and PABA was determined over a pH range of 5.5−10.0. The kinetics were determined with AcCoA as the variable substrate at a fixed, saturating concentration of PABA. As shown in Figure 5A, the value of k_{cat} increases as a function of pH, until a plateau is reached above pH 7.0. The data were best fit to a single curve, yielding a pK_a of 5.6 ± 0.1 and a $(k_{cat})_{lim}$ of 164 ± 5 s^{-1} (eq 15). Because the k_{cat} depends on both k_2 and k_4 (eq 7), the pK_a of 5.6 is considered as an apparent pK_a for the ionization of groups involved in either or both chemical reaction steps. The pH versus log(k_{cat}/K_{AcCoA}) profile revealed a bell-shape-like curve with two inflection points (Figure 5B). The value of log(k_{cat}/K_{AcCoA}) increased as a function of pH to a maximum at pH 7.0 and decreased until a plateau was reached above pH 8.5. The data were fit with eq 15 to yield a pK_{a_1} of 5.3 ± 0.1 and a pK_{a_2} of 8.5 ± 0.2, respectively. A value of 43 ± 3 mM^{-1} s^{-1} for $(k_{cat}/K_a)_{lim}$ was observed, and the ratio, *r*, for the two protonation states was found to be 0.33 ± 0.06. Generally, the pH dependence of k_{cat}/K_a reports the pK_a values for the ionization of groups on the free enzyme or free ligand involved in binding or catalysis in the first half of the reaction (*31*). Because there are no ionizable groups on AcCoA with pK_a values in the range of 5.3−8.5, both ionizable groups likely reside on NAT2. The value of pK_{a_1} is in good agreement with a previously reported apparent pK_a of 5.2 for the active-site thiolate−imidazolium ion pair (*20*). Because the k_{cat} is pH-independent at pH values above 7.0 (Figure 5A), the ionizable group with the pK_a of 8.5 is likely involved in AcCoA binding rather than in the chemical reaction.

The pH dependence of the transacetylation reaction with PNPA and PABA was monitored over a pH range of 5.2−9.0. The kinetic values were determined at a fixed PNPA concentration of 2 mM, while varying the PABA concentration. The pH versus k_{cat}/K_b data were plotted and fit to eq 16 to yield a pK_a of 5.5 ± 0.1 and a $(k_{cat}/K_b)_{lim}$ of 3000 ± 50 mM^{-1} s^{-1} (Figure 6). The ratio, *r*, was calculated to be 0.13 ± 0.04, indicating an approximate 8-fold increase of k_{cat}/K_b when the ionizable group is in its deprotonated form. Consistent with an *r* value approaching 0, however, no difference was observed between fits of the data to eqs 15 and 16 (see the Supporting Information). Consequently, the

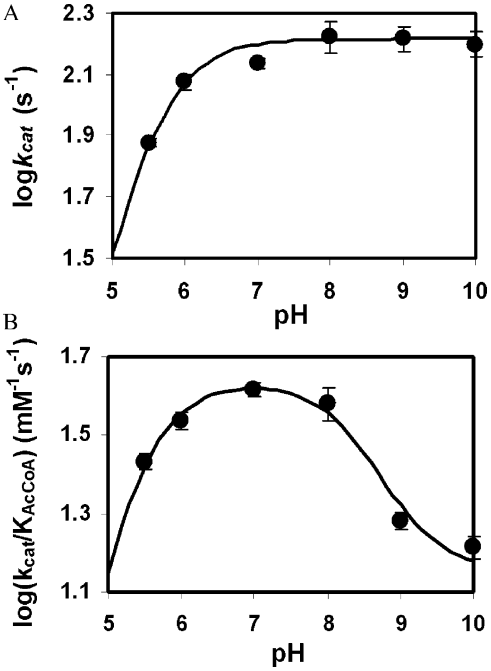

FIGURE 5: pH dependencies of the steady-state kinetic data for the transacetylation reaction of NAT2 with AcCoA and PABA. Reactions were conducted as described in the Materials and Methods. (A) Plot of log k_{cat} versus pH. The data were fit to eq 15, and the best-fit parameters are pK_a = 5.60 ± 0.08 and $(k_{cat})_{lim}$ = 160 ± 5 s^{-1}. (B) Plot of log(k_{cat}/K_{AcCoA}) versus pH. The data were fit to eq 17, and the best fit parameters are pK_{a_1} = 5.3 ± 0.1, pK_{a_2} = 8.5 ± 0.2, $(k_{cat}/K_{AcCoA})_{lim}$ = 43 ± 3 mM^{-1} s^{-1}, and *r* = 0.33 ± 0.06.

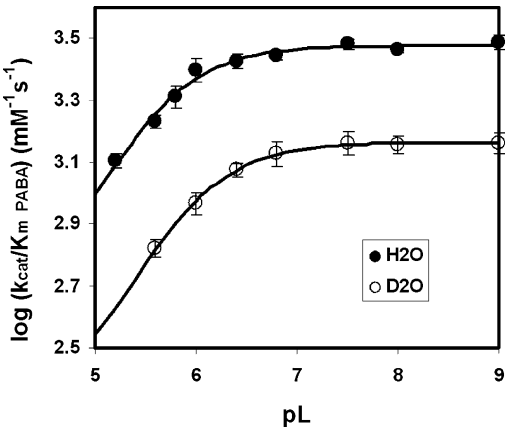

FIGURE 6: pL dependences of log(k_{cat}/K_{PABA}) for the transacetylation reaction of NAT2 with PNPA and PABA. Experiments were performed in H_2O (●) and 98% D_2O (○) as described in the Materials and Methods. The data were fit to eq 16, and the best-fit parameters are pK_a = 5.5 ± 0.1, *r* = 0.13 ± 0.04, and $(k_{cat}/K_{PABA})_{lim}$ = 3000 ± 50 mM^{-1} s^{-1} in H_2O and pK_a = 5.8 ± 0.1, *r* = 0.12 ± 0.02, and $(k_{cat}/K_{PABA})_{lim}$ = 1460 ± 10 mM^{-1} s^{-1} in 98% D_2O. The SKIE on k_{cat}/K_{PABA} was calculated as the ratio of $(k_{cat}/K_{PABA})_{lim}^{H}/(k_{cat}/K_{PABA})_{lim}^{D}$, which is 2.01 ± 0.04.

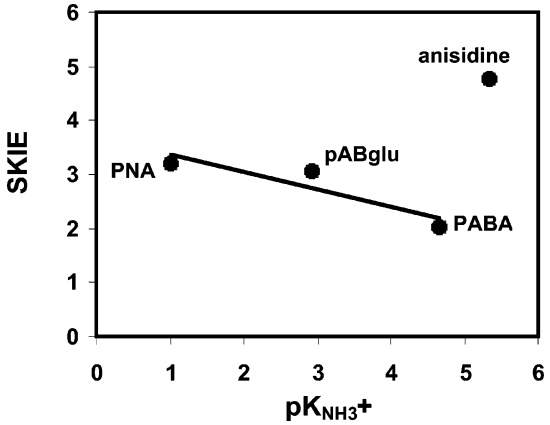

FIGURE 7: Plot of the SKIEs on k_{cat}/K_b versus the $pK_{NH_3^+}$ of the arylamines. Experiments were performed in H_2O and 98% D_2O as described in the Material and Methods. The k_{cat}/K_b is determined to be $^{H}(k_{cat}/K_{anisidine}) = 1190 \pm 30$ mM^{-1} s^{-1}, $^{D}(k_{cat}/K_{anisidine}) = 250 \pm 10$ mM^{-1} s^{-1}, $^{H}(k_{cat}/K_{pABglu}) = 95 \pm 1$ mM^{-1} s^{-1}, $^{D}(k_{cat}/K_{pABglu}) = 31 \pm 1$ mM^{-1} s^{-1}, $^{H}(k_{cat}/K_{PNA}) = 0.81 \pm 0.02$ mM^{-1} s^{-1}, and $^{D}(k_{cat}/K_{PNA}) = 0.25 \pm 0.01$ mM^{-1} s^{-1}. The SKIE on k_{cat}/K_b was calculated to be 4.8 ± 0.1, 3.1 ± 0.03, and 3.2 ± 0.05 for anisidine, pABglu, and PNA, respectively. Plotting the SKIE versus the corresponding $pK_{NH_3^+}$ of the arylamines, except anisidine, yields a slope of -0.32 and the squared correlation coefficient of 0.81.

8-fold increase of k_{cat}/K_b is likely only a lower limit of the effect of the deprotonated active-site group on k_{cat}/K_b. Similar to the pH versus k_{cat}/K_a profile, the pH versus k_{cat}/K_b profile reflects the pK_a of the ionization of groups on the acetyl−enzyme and/or PABA involved in substrate binding or catalysis in the second half of the reaction (*31*). Because the reported pK_a for the amine and carboxylate groups of PABA were found to be 4.67 and 2.5, respectively (*30*), the pK_a of 5.5 in the pH versus k_{cat}/K_b profile is assigned to ionization of a group on the acetyl−enzyme, which may function as a general base in the deacetylation step.

SKIEs. To assess the possibility of general base catalysis during the deacetylation reaction, the kinetic parameter, k_{cat}/K_b for PABA, was determined in reaction buffers composed of 98% D_2O over a pL range of 5.2−9.0. Reactions were carried out under the same experimental conditions as described above. The k_{cat}/K_b value was greater in H_2O than in D_2O at all pL values tested. Plotting the pD versus k_{cat}/K_b revealed a similar single curve (Figure 6). The inflection point of the curve was shifted by 0.32 units to 5.8 ± 0.1, consistent with a 0.4−0.6 unit shift toward basic pH generally observed in D_2O (*27*). Furthermore, because the $(k_{cat}/K_b)_{lim}$ is independent of pH, the ratio of $(k_{cat}/K_b)_{lim}$ in H_2O (3000 ± 50 mM^{-1} s^{-1}) versus in D_2O (1460 ± 10 mM^{-1} s^{-1}) corresponds to a normal solvent isotope effect $[^{H/D}(k_{cat}/K_b)_{lim}]$ of 2.01 ± 0.04, which supports a mechanism dependent on general base catalysis.

The solvent isotope effect on the deacetylation rate was also examined at pL 7.0 with anisidine, pABglu, and PNA as the acetyl acceptors. Reactions were performed at a fixed concentration of either PNPA (2 mM) or AcCoA (400 μM) while varying the arylamine concentration. The second-order rate constant values (k_{cat}/K_b) for anisidine, pABglu, and PNA were calculated from the Lineweaver−Burk plots. The ratio of the k_{cat}/K_b in H_2O versus in 98% D_2O yielded a normal solvent isotope effect of $[^{H/D}(k_{cat}/K_b)]$ of 4.8 ± 0.1 for anisidine, 3.1 ± 0.03 for pABglu, and 3.2 ± 0.05 for PNA (Figure 7).

pH Effects on Acetyl−Enzyme Hydrolysis. To investigate the possible general base catalysis during the acetyl−enzyme hydrolysis, the pH dependence of the acetyl−enzyme hydrolysis reaction was determined at a fixed PNPA concentration of 320 μM and over a pH range of 5.2−9.0. Because previous stopped-flow kinetics demonstrated that the rate of acetylation (k_2[PNPA]) in the presence of 320 μM of PNPA is much faster than the rate of acetyl−enzyme hydrolysis (k_{H_2O}), the steady-state initial velocity represents the k_{H_2O} (*20*). The k_{H_2O} is independent of pH within the pH range of 5.2−7.5, while a 3-fold increase in the k_{H_2O} is observed at pH 9.0 (see the Supporting Information). The hydroxide group, acting as a more reactive nucleophile than H_2O, is likely to be responsible for the increase in the hydrolysis rate under the basic conditions. The data suggest that, unlike the deacetylation of acetyl−enzyme with arylamine substrates, no kinetically observable general base catalysis is involved in acetyl−enzyme hydrolysis at neutral pH.

Site-Directed Mutagenesis of H107Q and H107N. According to SDS−PAGE and Western blots of cell lysates, only the H107Q mutant was overexpressed in the Rosetta cell line. However, neither H107N nor H107Q NAT2 was found to be expressed in the BL21(RIL) cell line. The overexpressed H107Q mutant was found predominantly in the insoluble fraction of the cell lysate, and no transacetylase activity was observed in the soluble fraction. Because the wild-type NAT2 from the insoluble protein can be successfully refolded, with an activity of at least 25−50% of the fusion protein activity (*20*), the same refolding procedure was applied to the H107Q mutant. The refolded and soluble mutant protein, however, was found to be devoid of transacetylase activity at pH 7.0 and 8.5 (data not shown).

DISCUSSION

Despite their discovery by Lippman and co-workers over 50 years ago and their later identification as important mediators of drug and xenobiotic metabolism, a full understanding of the catalytic mechanism and natural function of NATs has remained elusive (*32*). Nevertheless, crystallographic, kinetic, and molecular biological studies are beginning to clarify the biochemical and biological role of NATs (*20*, *21*, *33*, *34*).

Catalysis by NATs has been shown to rely on a bi-bi ping-pong mechanism characterized by acetylation with AcCoA or an acetylated phenol of a strictly conserved active-site cysteine, followed by transfer of an acetyl group to an arylamine acceptor. On the basis of substrate specificity studies with acetylated phenols and aniline donors and acceptors, Jencks and co-workers suggested that the acetyl transfer reaction is likely facilitated by general acid−base catalysis in which a partial positive charge develops on the nitrogen of the arylamine (*20*, *35*). In addition, depending on the basicity of the arylamine, the rate-determining step for the reaction could be shifted from enzyme acetylation to deacetylation. Subsequent substrate specificity studies with AcCoA by Weber and co-workers confirmed this conclusion for rabbit NAT (*36*).

Recently, structural and mechanistic studies have begun to provide the first detailed explanation of the catalytic mechanism of NATs. X-ray crystallographic studies of the *Salmonella typhimurium* NAT revealed that the previously

identified active-site cysteine was part of a catalytic cysteine-histidine-aspartic triad (*21*). Sequence alignment studies of both prokaryote and eukaryote NATs suggest that the triad is an essential part of the catalytic machinery of the enzyme. Kinetic, alkylation, and mutagenic studies of the acetylation of hamster NAT2 by our laboratory have demonstrated that (1) catalysis is governed by a thiolate imidazolium ion pair with a pK_a of 5.16, (2) the triad His-107 is solvent-inaccessible with an apparent pK_a > 9.0, (3) the enzyme protects the active-site thiol ester intermediate from hydrolysis, (4) the pK_a of His-107 in the acetylated enzyme must be well below pH 7, (5) a pH-dependent conformational change is responsible for the second pK_a and not His-107, and (6) Asp-122 is necessary for optimal enzymatic activity and structural stability (*20*). Although these results are informative, a complete understanding of NAT catalysis requires that the deacylation step be fully described. Consequently, we have chosen to investigate the second half of the transferase reaction by steady-state kinetics, SKIE studies, and site-directed mutagenesis.

Steady-State Kinetic Analysis. To delineate the factors governing the arylamine N-acetylation by hamster NAT-2, we determined the steady-state parameters for the acetylation with both PNPA and AcCoA. As can be seen in Table 1, the k_{cat}/K_a values are relatively close and similar to the second-order rate constant of (140 ± 5) mM^{-1} s^{-1} previously observed by transient kinetic analysis (*20*). In contrast to the results reported for avian NAT, PNPA behaves like an acetylation reagent (*20*, *35*). With AcCoA, however, saturation is observable; thus, k_{cat}/K_{AcCoA} is dependent on AcCoA binding. This is clearly evident from the pH versus k_{cat}/K_{AcCoA} profile, in which two pK_a values were revealed (Figure 5B). The pK_{a_1} values for enzyme acetylation with either PNPA or AcCoA are in good agreement (5.16 versus 5.32) (*20*). On the basis of an observed inverse SKIE for both enzyme alkylation and acetylation, pK_{a_1} has been assigned to a catalytically necessary active-site thiolate−imidazolium ion pair, while a pH-dependent conformational change is likely responsible for pK_{a_2} (6.79) (*20*). In contrast, for AcCoA, pK_{a_2} (8.48) is nearly 2 pH units greater than the value observed for PNPA. This discrepancy is not the result of a shift in the pH dependence of a protein conformational change but is due to the pH dependence observed for the cofactor apparent K_m (K_{AcCoA}) (data not shown). Because we have previously established that the pK_a for the histidine of the thiolate−immidazole ion pair is >9 and a second pK_a is not observed for the overall rate (k_{cat}) of PABA acetylation, it is likely that pK_{a_2} reflects the pK_a of a residue involved in AcCoA binding.

On the basis of our previous pre-steady-state kinetic analysis, the pK_a for His-107 after thiolate acetylation, must be shifted from a value >9 to a value similar to that observed for the thiolate−imidazolium ion pair (pK_a = 5.16) (*20*). Examination of the pH versus k_{cat}/K_{PABA} profile for PNPA and PABA (Figure 6) revealed a dependence on a single nearly identical pK_a value (5.5). Because only the effect on deacetylation is considered under these conditions, the observation of a normal SKIE across the entire pH range for the pH versus k_{cat}/K_{PABA} profile for PNPA and PABA demonstrates that arylamine enzyme deacetylation is dependent on general base catalysis. Consequently, we have assigned the pK_a for His-107 for the acetylated enzyme to be 5.5, which, as predicted, is similar to the pK_a of 5.16 for the nonacetylated enzyme.

When we turn now to the transferase reaction, the k_{cat} values for each of the three arylamines, when determined with PNPA, are equivalent to the rate of enzyme deacetylation (k_4, eq 2). Clearly, the rate of deacetylation by PABA is >5- and 3-fold greater than the rate observed for pABglu and anisidine, respectively. Because the enzyme is able to form a Michaelis−Menten complex with AcCoA, the k_{cat} values determined with the cofactor are composed of both the rate of enzyme acetylation (k_2, eq 7) and deacetylation (k_4, eq 7). However, when the reaction is carried out with PNA, enzyme deacetylation becomes almost entirely rate-limiting. Therefore, k_{cat} for PNA is the true enzyme deacetylation rate (k_4) for this substrate, and the K_b is the true K_m^b. In principle, one could calculate the acetylation rate constant for AcCoA based on knowing the k_4 value for PNA. However, because the k_{cat} value is small, a unique value for the rate of enzyme acetylation cannot be determined. Nevertheless, when PNPA is the substrate, the rate of PABA deacetylation (k_4) is equivalent to k_{cat} and the value of k_2 (300 s^{-1}) for AcCoA can be calculated (eq 7). In addition, when we know the K_b for PABA, obtained with AcCoA, the K_m^b value for PABA obtained with PNPA, and the rate of deacetylation (k_4) for PABA, a value for the rate of enzyme acetylation by AcCoA (650 s^{-1}) can be calculated (eq 9). Consequently, we have determined that the rate of enzyme acetylation falls within a range of 300−650 s^{-1}, with an average value of 480 s^{-1}. Substitution of the value for the rate of enzyme acetylation by AcCoA and the value for the rate of enzyme deacetylation by PABA into eq 8 allows for the K_m^a for AcCoA (5.90 mM) to be ascertained. The validity of these assumptions appears justified because utilizing the k_2 value of 480 s^{-1} and the corrected k_4 value of 160 s^{-1} for pABglu results in a predicted k_{cat} value (94 s^{-1}) that is similar to the experimental value (76 s^{-1}) for acetylation of the enzyme by AcCoA.

Although the k_4 values for the arylamine substrates indicate that PABA is the preferred substrate, a comparison of the specificities typically relies on k_4/K_m^b data. When PNPA is used as a substrate, K_b becomes equivalent to the K_m^b (eq 4) for the arylamine acceptor; thus, k_{cat}/K_b is equivalent to the substrate specificity constant, k_4/K_m^b (eq 5). On the basis of this analysis, PABA is preferred over pABglu, by nearly 40-fold. Similar to results obtained with PNPA, PABA again emerges as the preferred substrate over pABglu and PNA by a factor of at least 50 and 2200, respectively, when the reaction is carried out with AcCoA. Consequently, regardless of the acetylation substrate, the enzyme specificity is dependent upon changes in both the k_{cat} and K_m for the arylamine.

Linear Free-Energy Relationships (LFERs). While steady-state analysis has delineated the sequence of events and likely participation of enzyme acetylation and deacetylation in the overall rate of hamster NAT2 catalysis, the use of LFERs coupled to SKIE studies can provide a detailed picture of the catalytic mechanism (*37*). Brønsted plots, in particular, can provide valuable insights into the nature of the chemical step (*35*). Previously, Jencks and co-workers demonstrated a positive β_{nuc} parameter of 0.6 for the acetylation of a subset of arylamines by pigeon liver arylamine *N*-acetyltransferase (*35*). This was interpreted as evidence of the build up of

Scheme 3: Proposed Mechanism of the NAT2 Catalyzed Transacetylation Reaction

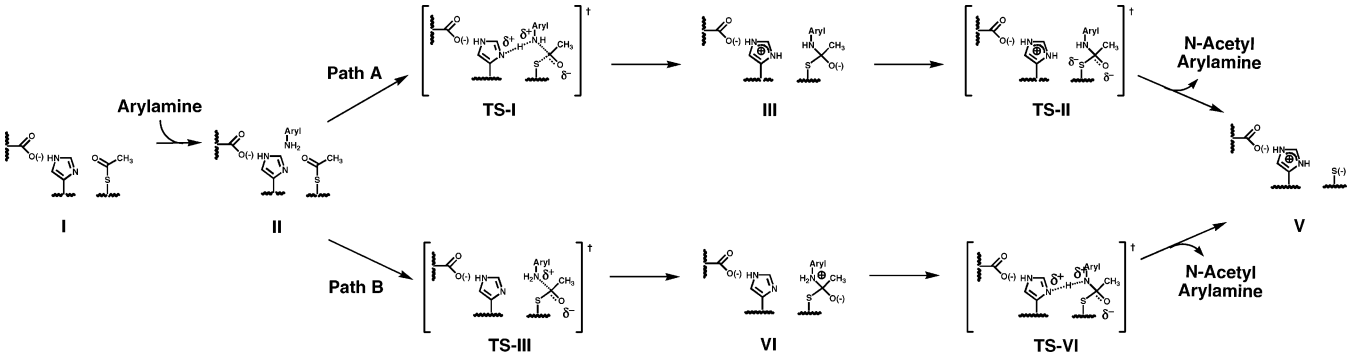

positive charge on the nucleophilic nitrogen, which is reduced by significant proton abstraction by an active-site base. If the values for anisidine are excluded, a plot of the log of the rate of enzyme deacetylation versus arylamine pK_a revealed a similar positive β_{nuc} parameter of 0.8 ± 0.1 for hamster NAT2. The fact that the value approaches unity indicates that the rate of enzyme deacetylation and the protonation equilibrium constant of the nucleophile are nearly equally sensitive to substrate substituent effects. In contrast to the pigeon enzyme, a substantial amount of bond formation between the nitrogen and the carbonyl is found in the transition state for hamster NAT2, while proton removal remains less significant. The β_{nuc} value is similar, however, to the value (β_{nuc} = 0.9) found for the nonenzymatic aminolysis of model thiol esters (*38*). Thus, the enzymatic reaction does not attempt to reduce the charge build up on the nitrogen in the transition state but to maximize utilization of substrate nucleophilicity (path A in Scheme 3).

Although the rate of deacetylation by anisidine is only 43% of that found for PABA, given the pK_a of anisidine, the rate would have been predicted to be at least an order of magnitude greater. Deviation from linearity for the Brønsted plot was also observed for pigeon NAT (*35*). Because a K_m could be observed for PNPA with pigeon NAT, this phenomenon was found to result from a change, with increasing arylamine nucleophilicity, in the rate-limiting step from enzyme deacetylation to acetylation. This is not the case for hamster NAT2, because PNPA behaves as an acetylation reagent and not a substrate.

To address the nature of the discrepancy between anisidine and the other substrates, we decided to probe the structure of the transition states for enzyme deacetylation by determining the SKIE for each arylamine. The reactions were carried out at the plateau region of the pH rate profile, ensuring complete enzyme and substrate deuteration. One could envision three possible scenarios for a SKIE versus pK_a plot. First, if a slope (ΔSKIE/ΔpK_a) of zero is observed, then the rate-limiting step would be dependent on arylamine nucleophilicity and not proton removal by an active-site base. Second, if a negative slope of 1 is observed, then the rate-limiting step would be dependent on proton removal by an active-site base and not substrate nucleophilicity. Third, if the slope is > -1 but <0, then the rate-limiting step must be dependent on some degree of arylamine nucleophilicity and active-site-assisted proton removal. In the latter case, a value closer to -1 would be more influenced by proton removal, while a value closer to zero will be more dependent on substrate nucleophilicity. As can be seen in Figure 7, a linear relationship is observed for a plot of the SKIE versus pK_a for PNA, PABA, and pABglu with a negative and shallow slope (-0.32). This result is consistent with the conclusion from the Brønsted plot analysis that the transition state must be characterized by the build up of partial positive charge on the nucleophilic nitrogen, before proceeding through an enzyme-bound tetrahedral intermediate.

This correlation that we observed for PNA, PABA, and pABglu does not apply to the most nucleophilic and least acidic arylamine, anisidine. The observed SKIE of 4.47 for anisidine differs significantly from the predicted SKIE of 1.97. In fact, the observed deacetylation rate ($k_4 = 260\ s^{-1}$) is nearly 10^7-fold greater than the rate ($k_4 = 3.3 \times 10^{-5}\ s^{-1}$) predicted for the observed SKIE of 4.5. This finding can be easily rationalized, however, if enzyme deacetylation by anisidine is a stepwise process (path B in Scheme 3). Rapid formation of a tetrahedral intermediate, followed by rate-limiting proton transfer to the active-site base, is consistent with the divergence between the observed and predicted SKIE (Figure 7). Not surprisingly, this mechanistic change occurs almost precisely at the pK_a of the active-site base. Thus, relative to PNA, pABglu, and anisidine, PABA appears to be the best substrate in part because of its optimal nucleophilicity and pK_a. Studies of structurally different arylamines with pK_a values similar to PABA will delineate the potential importance of active-site binding on catalysis.

SUMMARY AND CONCLUSIONS

On the basis of our earlier evaluation of the acetylation and alkylation of NAT2, we concluded that the active site contains a highly reactive thiolate−imidazolium with a pK_a of 5.2 (*20*). In contrast to cysteine proteases, the proton shared by the thiolate and imidazolium (pK_a > 9.0) is difficult to remove, even under basic conditions. This is likely a reflection of the location of the triad at the bottom of a deep nonpolar pocket and the positioning of the imidazole between Asp-122 and Cys-68. The inability of the enzyme to accommodate even a sterically and electronically similar mutation at this position supports this hypothesis. Once the thiolate is acetylated, however, half of the ion pair is lost, with a concomitant shift in the pK_a of His-107 to 5.5. Consequently, under physiological conditions, the imidazole is poised to facilitate proton transfer from the developing deacetylation transition state if the arylamine is a sufficiently weak nucleophile with a pK_a < 5.5. Strong nucleophiles with pK_a values ≥5.5 result in a mechanistic shift from a process dominated by nucleophilic attack of the thiol ester (path A in Scheme 3), to deprotonation of a tetrahedral intermediate

(path B in Scheme 3). While both a concerted and stepwise mechanism are consistent with path A for arylamines with pK_a values less than 5.5, formation of an unstable tetrahedral intermediate is consistent with path B and does not necessitate a more distinct process. Efficient deacetylation, therefore, depends on an optimal balance between the free energy of the equilibrium for proton transfer and amide bond formation. PABA apparently fulfills this requirement, while pABglu, PNA, and anisidine do not.

The prominent role played by the NATs in the metabolism of xenobiotic arylamines is well-established. Certain fundamental questions, however, arise from our mechanistic conclusions for hamster NAT2. First, because an endogenous cellular function for NATs has not been definitively elucidated and only a fraction of excreted pABglu is acetylated, the remarkable preference of hamster NAT2 and human NAT1 for PABA as a substrate suggests that, in addition to folate catabolism, a novel biochemical role may exist for PABA and acetylated PABA. Second, on the basis of sequence analysis studies, hamster NAT1 and NAT2 rely on the same catalytically necessary triad. Nevertheless, anisidine and not PABA is the preferred substrate for NAT1. How these highly homologous isoenzymes accommodate this change in substrate specificity is not apparent. Clearly, this variability must be the result of differing nucleophilic and pK_a requirements for catalysis. Key interactions between the substrate and the enzyme active site are also likely to play a role in substrate specificity, but the exact nature of these interactions and the extent of their contribution remains to be determined (*34*). In addition, our recent observation that the lifetime for acetylated hamster NAT2 is 9-fold greater than the lifetime for acetylated hamster NAT1 probably reflects a certain degree of mechanistic diversity for NATs (*39*). Ongoing comparative enzymological studies of NATs should address these questions, thus enhancing our understanding of their cellular function.

SUPPORTING INFORMATION AVAILABLE

Fits to pL dependences of $\log(k_{cat}/K_{PABA})$ for the transacetylation reaction of NAT2 with PNPA and PABA based on eqs 15 and 16 (Figure S1). pH dependence of acetyl−enzyme hydrolysis by water (Figure S2). This material is available free of charge via the Internet at http://pubs.acs.org.

REFERENCES

1. Hanna, P. E. (1994) *N*-acetyltransferases, *O*-acetyltransferases, and *N*,O-acetyltransferases: Enzymology and bioactivation, *Adv. Pharmacol. 27*, 401−430.
2. Hanna, P. E. (1996) Metabolic activation and detoxification of arylamines, *Curr. Med. Chem. 3*, 195−210.
3. Levy, G. N., and Weber, W. W. (2002) in *Enzyme Systems That Metabolise Drugs and Other Xenobiotics* (Ioaniddes, C., Ed.) pp 441−457, John Wiley and Sons, New York.
4. Hein, D. W., Grant, D. M., and Sim, E. (2000) Update on consensus arylamine *N*-acetyltransferase gene nomenclature, *Pharmacogenetics 10*, 291−292.
5. Grant, D. M., Blum, M., Beer, M., and Meyer, U. A. (1991) Monomorphic and polymorphic human arylamine *N*-acetyltransferases: A comparison of liver isozymes and expressed products of two cloned genes, *Mol. Pharmacol. 39*, 184−191.
6. Hein, D. W., Doll, M. A., Fretland, A. J., Leff, M. A., Webb, S. J., Xiao, G. H., Devanaboyina, U. S., Nangju, N. A., and Feng, Y. (2000) Molecular genetics and epidemiology of the NAT1 and NAT2 acetylation polymorphisms, *Cancer Epidemiol., Biomarkers Prev. 9*, 29−42.
7. Upton, A., Johnson, N., Sandy, J., and Sim, E. (2001) Arylamine *N*-acetyltransferases of mice, men, and microorganisms, *Trends Pharmacol. Sci. 22*, 140−146.
8. Ohsako, S., and Deguchi, T. (1990) Cloning and expression of cDNAs for polymorphic and monomorphic arylamine *N*-acetyltransferases from human liver, *J. Biol. Chem. 265*, 4630−4634.
9. Stanley, L. A., Copp, A. J., Pope, J., Rolls, S., Smelt, V., Perry, V. H., and Sim, E. (1998) Immunochemical detection of arylamine *N*-acetyltransferase during mouse embryonic development and in adult mouse brain, *Teratology 58*, 174−182.
10. Irshaid, Y. M., al-Hadidi, H. F., Abuirjeie, M. A., Rawashdeh, N. M., and Gharaibeh, N. S. (1993) Acetylation of dapsone by human whole blood, *Int. J. Clin. Pharmacol. Ther. Toxicol. 31*, 18−22.
11. Pacifici, G. M., Bencini, C., and Rane, A. (1986) Acetyltransferase in humans: Development and tissue distribution, *Pharmacology 32*, 283−291.
12. Rodrigues-Lima, F., Cooper, R. N., Goudeau, B., Atmane, N., Chamagne, A. M., Butler-Browne, G., Sim, E., Vicart, P., and Dupret, J. M. (2003) Skeletal muscles express the xenobiotic-metabolizing enzyme arylamine *N*-acetyltransferase, *J. Histochem. Cytochem. 51*, 789−796.
13. Sim, E., Pinter, K., Mushtaq, A., Upton, A., Sandy, J., Bhakta, S., and Noble, M. (2003) Arylamine *N*-acetyltransferases: A pharmacogenomic approach to drug metabolism and endogenous function, *Biochem. Soc. Trans. 31*, 615−619.
14. Dyda, F., Klein, D. C., and Hickman, A. B. (2000) GCN5-related *N*-acetyltransferases: A structural overview, *Annu. Rev. Biophys. Biomol. Struct. 29*, 81−103.
15. Minchin, R. F. (1995) Acetylation of *p*-aminobenzoylglutamate, a folic acid catabolite, by recombinant human arylamine *N*-acetyltransferase and U937 cells, *Biochem. J. 307* (part 1), 1−3.
16. McPartlin, J., Courtney, G., McNulty, H., Weir, D., and Scott, J. (1992) The quantitative analysis of endogenous folate catabolites in human urine, *Anal. Biochem. 206*, 256−261.
17. Hein, D. W., Doll, M. A., Fretland, A. J., Gray, K., Deitz, A. C., Feng, Y., Jiang, W., Rustan, T. D., Satran, S. L., and Wilkie, T. R., Sr. (1997) Rodent models of the human acetylation polymorphism: Comparisons of recombinant acetyltransferases, *Mutat. Res. 376*, 101−106.
18. Kato, R., and Yamazoe, Y. (1995) Molecular mechanisms of polymorphism in acetylating enzymes for arylamines and *N*-hydroxyarylamines in hamster liver, *Drug Metab. Rev. 27*, 241−256.
19. Vatsis, K. P., Weber, W. W., Bell, D. A., Dupret, J. M., Evans, D. A., Grant, D. M., Hein, D. W., Lin, H. J., Meyer, U. A., Relling, M. V. et al. (1995) Nomenclature for *N*-acetyltransferases, *Pharmacogenetics 5*, 1−17.
20. Wang, H., Vath, G. M., Gleason, K. J., Hanna, P. E., and Wagner, C. R. (2004) Probing the mechanism of hamster arylamine *N*-acetyltransferase 2 acetylation by active site modification, site-directed mutagenesis, and pre-steady state and steady-state kinetic studies, *Biochemistry 43*, 8234−8246.
21. Sinclair, J. C., Sandy, J., Delgoda, R., Sim, E., and Noble, M. E. (2000) Structure of arylamine *N*-acetyltransferase reveals a catalytic triad, *Nat. Struct. Biol. 7*, 560−564.
22. Rodrigues-Lima, F., and Dupret, J. M. (2002) 3D model of human arylamine *N*-acetyltransferase 2: Structural basis of the slow acetylator phenotype of the R64Q variant and analysis of the active-site loop, *Biochem. Biophys. Res. Commun. 291*, 116−123.
23. Rodrigues-Lima, F., Delomenie, C., Goodfellow, G. H., Grant, D. M., and Dupret, J. M. (2001) Homology modelling and structural analysis of human arylamine *N*-acetyltransferase NAT1: Evidence for the conservation of a cysteine protease catalytic domain and an active-site loop, *Biochem. J. 356*, 327−334.
24. Bradford, M. M. (1976) A rapid and sensitive method for the quantitation of microgram quantities of protein utilizing the principle of protein−dye binding, *Anal. Biochem. 72*, 248−254.
25. Sticha, K. R., Sieg, C. A., Bergstrom, C. P., Hanna, P. E., and Wagner, C. R. (1997) Overexpression and large-scale purification of recombinant hamster polymorphic arylamine *N*-acetyltransferase as a dihydrofolate reductase fusion protein, *Protein. Expression Purif. 10*, 141−153.
26. Ward, A., Hickman, D., Gordon, J. W., and Sim, E. (1992) Arylamine *N*-acetyltransferase in human red blood cells, *Biochem. Pharmacol. 44*, 1099−1104.
27. Schowen, K. B., and Schowen, R. L. (1982) Solvent isotope effects of enzyme systems, *Methods Enzymol. 87*, 551−606.

28. Ellis, K. J., and Morrison, J. F. (1982) Buffers of constant ionic strength for studying pH-dependent processes, *Methods Enzymol. 87*, 405−426.
29. Scott, I. A. (1964) *Interpretation of the Ultraviolet Spectra of Natural Products*, Macmillan, New York.
30. Perrin, D. D. (1965) *Dissociation Constants of Organic Bases in Aqueous Solutions*, Butterworths, London, U.K.
31. Fersht, A. (1999) *Structure and Mechanism in Protein Science: A Guide to Enzyme Catalysis and Protein Folding*, W. H. Freeman, New York.
32. Chou, T. C., and Lipmann, F. (1952) Separation of acetyl transfer enzymes in pigeon liver extract, *J. Biol. Chem. 196*, 89−103.
33. Sandy, J., Mushtaq, A., Kawamura, A., Sinclair, J., Sim, E., and Noble, M. (2002) The structure of arylamine *N*-acetyltransferase from *Mycobacterium smegmatis*—An enzyme which inactivates the anti-tubercular drug, isoniazid, *J. Mol. Biol. 318*, 1071−1083.
34. Goodfellow, G. H., Dupret, J. M., and Grant, D. M. (2000) Identification of amino acids imparting acceptor substrate selectivity to human arylamine acetyltransferases NAT1 and NAT2, *Biochem. J. 348* (part 1), 159−166.
35. Riddle, B., and Jencks, W. P. (1971) Acetyl-coenzyme A: Arylamine *N*-acetyltransferase. Role of the acetyl-enzyme intermediate and the effects of substituents on the rate, *J. Biol. Chem. 246*, 3250−3258.
36. Weber, W. W., and Cohen, S. N. (1967) *N*-Acetylation of drugs: Isolation and properties of an *N*-acetyltransferase from rabbit liver, *Mol. Pharmacol. 3*, 266−273.
37. Leblanc, A., Gravel, C., Labelle, J., and Keillor, J. W. (2001) Kinetic studies of guinea pig liver transglutaminase reveal a general-base-catalyzed deacylation mechanism, *Biochemistry 40*, 8335−8342.
38. Castro, E. A., and Ureta, C. (1989) Structural-reactivity correlation in the aminolysis of phenyl and *p*-nitrophenyl thiolacetates, *J. Org. Chem. 54*, 2153−2159.
39. Wang, H., Wagner, C. R., and Hanna, P. E. (2005) Irreversible interaction of arylamine *N*-acetyltransferases in the presence of *N*-hydroxy-4-acetylaminobiphenyl: A comparison of human and hamster enzymes, *Chem. Res. Toxicol. 18*, 183−197.

BI047564Q